Available online at www.sciencedirect.com
SCIENCE DIRECT®
Biomaterials 27 (2006) 905–916
Biomaterials
www.elsevier.com/locate/biomaterials

Architecture and properties of anisotropic polymer composite scaffolds for bone tissue engineering

Laurence Marcelle Mathieu[a,c], Thomas L. Mueller[b], Pierre-Etienne Bourban[a], Dominique P. Pioletti[c,d], Ralph Müller[b], Jan-Anders E. Månson[a,*]

[a]*Laboratoire de Technologie des Composites et Polymères (LTC), Ecole Polytechnique Fédérale de Lausanne (EPFL), CH-1015 Lausanne, Switzerland*
[b]*Institute for Biomedical Engineering, Swiss Federal Institute of Technology (ETH) and University of Zürich, CH-8044 Zürich, Switzerland*
[c]*Laboratoire de Recherche en Orthopédie (LRO), Ecole Polytechnique Fédérale de Lausanne (EPFL), CH-1015 Lausanne, Switzerland*
[d]*Hôpital Orthopédique de la Suisse Romande, CH-1005 Lausanne, Switzerland*

Received 8 December 2004; accepted 5 July 2005
Available online 27 July 2005

Abstract

Bone is a complex porous composite structure with specific characteristics such as viscoelasticity and anisotropy, both in morphology and mechanical properties. Bone defects are regularly filled with artificial tissue grafts, which should ideally have properties similar to those of natural bone. Open cell composite foams made of bioresorbable poly(L-lactic acid) (PLA) and ceramic fillers, hydroxyapatite (HA) or β-tricalcium phosphate (β-TCP), were processed by supercritical CO_2 foaming. Their internal 3D-structure was then analysed by micro-computed tomography (μCT), which evidenced anisotropy in morphology with pores oriented in the foaming direction. Furthermore compressive tests demonstrated anisotropy in mechanical behaviour, with an axial modulus up to 1.5 times greater than the transverse modulus. Composite scaffolds also showed viscoelastic behaviour with increased modulus for higher strain rates. Such scaffolds prepared by gas foaming of polymer composite materials therefore possess suitable architecture and properties for bone tissue engineering applications.

Keywords: Composite; Scaffold; Compression; MicroCT; Anisotropy

1. Introduction

Bone is a natural complex porous composite with unique properties of remodelling to adapt its micro-structure to external mechanical stress. Bone is also one of the tissues with the highest demand for tissue reconstruction or replacement [1]. Artificial tissue grafts were recently considered in order to overcome limitations of traditional allo- or autografts, such as risk of immune rejection and pathogen transfer, pain and infection, or limited availability [2]. Bioresorbable scaffolds, i.e. porous constructs, seeded with the appropriate type of cells, should provide a template for tissue regeneration, while slowly resorbing, to finally leaving no foreign substances in the body, thus reducing the risk of inflammation [3].

Scaffolds were initially composed of either polymer or ceramic, which, however, tended to be too flexible or too brittle, respectively. In the past few years, polymer/ceramic composites have therefore gained increased interest in the field of tissue engineering [4–7], to reconstruct several types of structural tissues, such as bone, cartilage, tendons or ligaments, and tissue interfaces. The composite is expected to have improved mechanical properties compared to the neat polymer, and better structural integrity and flexibility than brittle ceramics. In fact the combination of ceramic and polymer could provide reinforced porous structures

*Corresponding author. Tel.: +41 21 693 42 81; fax: +41 21 693 58 80.
E-mail address: jan-anders.manson@epfl.ch (J.-A.E. Månson).

0142-9612/$ - see front matter © 2005 Elsevier Ltd. All rights reserved.
doi:10.1016/j.biomaterials.2005.07.015

with enhanced bioactivity and controlled resorption rates [8].

Many studies have tried to define which properties are required for an optimal synthetic scaffold, in particular for bone tissue replacement [2,9–16]. They state that scaffolds need to be biocompatible. A three-dimensional (3D) internal geometry, similar to bone morphology, and the retention of mechanical properties after implantation are required for scaffolds in order to maintain a tissue space of prescribed size and shape for tissue formation. A porosity higher than 75% seems to be necessary. In the case of ceramic scaffolds, a macroporosity of 200–400 μm is needed to promote bone cell attachment, and a microporosity of less than 10 μm should promote ion and liquid diffusion [17]. Nevertheless, when using polymers, the pore size was not shown to be significant [18–20]. In the case of cancellous bone, anisotropic and viscoelastic mechanical behaviour, with a modulus of 300–500 MPa and a strength of 5–10 MPa, is desirable. These properties should be maintained long enough prior to degradation, i.e. till the newly grown tissue is capable of taking the load.

Scaffolds have been processed by several techniques. Solvent casting/particulate leaching [4,21] results in thin scaffolds with a well controlled interconnected porosity and pore size, and a compressive modulus of 0.15–150 MPa. Emulsion freeze-drying or thermally induced phase separation [22–25] lead to pore size between 20 and 100 μm, with a compressive modulus up to 20 MPa in the longitudinal direction. 3D-printing [2] requires the use of a complex and specific equipment. None of the previous methods were ideal for bone tissue engineering scaffolds, which often lacked mechanical resistance, with modulus under the minimum of cancellous bone. Moreover, the use of organic solvents is their common drawback. Although the latter are extensively used in the biomedical field, for scaffold fabrication, as reviewed previously, as well as to introduce proteins or other bioactive factors into polymer supports [26], they present a potential toxicity [27] which cannot be neglected.

Gas foaming was selected as a solvent-free process, which allows functional fillers to be added. Here, the latter consist in reinforcing ceramic particles, with osteoconductive properties. If foaming was carried out at room temperature, bioactive fillers could be directly added to the scaffold during processing [28]. In our case, these factors, if needed, can be added in a second step, when bringing cells to the porous structure. Moreover, a previous study has stressed the potential and flexibility of supercritical gas foaming to produce scaffolds with controlled architecture and properties [29].

The objective of this study was to characterise bioresorbable porous composites processed by supercritical CO_2 foaming. Microarchitectural parameters were evaluated by micro-computed tomography (μCT). This non-destructive technique, extensively used to characterise bone specimens [30,31], is based on X-ray radiation and started to be used for polymer foams [32–36]. The mechanical behaviour was tested in compression in order to evaluate anisotropy and viscoelasticity of prepared porous composite structures.

2. Materials and methods

2.1. Materials and scaffold processing

A commercial bioresorbable polymer, poly L-lactic acid (PLA; Boehringer Ingelheim, Germany) was used without further purification. It was characterised by an intrinsic viscosity of 1.6 dL/g and a melting temperature of 181.7 °C. Two ceramic powders were added to PLA: hydroxyapatite (HA) and β-tricalcium phosphate (β-TCP) (Dr. Robert Mathys Foundation, Switzerland). HA particles were of nanometric size, with a high specific surface area (50 m^2/g), while β-TCP particles were of micrometric size, with a much smaller specific surface area (1–2 m^2/g). Both PLA and ceramics were dried overnight at 105 °C under vacuum prior to use in order to prevent polymer degradation by hydrolysis. Foaming was carried out with supercritical CO_2 (pure > 99.995%; SL gas, Switzerland).

Ceramic fillers and polymer must be intimately mixed before the foaming process. Melt extrusion was shown to disperse homogeneously particles within the matrix without significant deterioration of the polymer, and without using any solvent [37]. PLA pellets and ceramic particles were first mixed in the dry state, then melt extruded with a micro-compounder (Micro 5 Compounder; DSM, The Netherlands) with two conical co-rotating screws, of small capacity (5 cm^3). Compounding was carried out under a flow of nitrogen to limit polymer degradation, with a set temperature of 205 °C, a screw rotation speed of 100 rpm and a residence time of 4 min, determined as the optimum mixing conditions in a previous study [37].

The supercritical gas foaming technique and equipment used in this work are described in detail in another article [38]. The foaming equipment was composed of a custom made high pressure chamber (Autoclave France, France) and a computerised data acquisition system. Samples, i.e. extruded rods, were put into cylindrical open moulds, 35 mm inner diameter, and loaded in the pressure vessel. Pressure was increased up to saturation pressure P_{sat} (150–250 bar), and temperature increased up to 195 °C, above the PLA melting point. On the opposite to amorphous PLGA as used by Howdle et al. [28], CO_2 diffuses slowly at or close to room temperature in semi-crystalline PLA. The latter must therefore be melted in order to accelerate this diffusion and increase CO_2 solubility in the polymer. Polymer saturation by CO_2 was completed after 10 min and a melt polymer—gas solution is created. Foaming was then achieved by sudden gas release, which induced the generation of nuclei due to supersaturation. These nuclei grew to form the porous structure. Initial depressurisation rate dP/dt, controlled by a back-pressure regulator, and maximum cooling rate dT/dt were found to be significant parameters affecting pore expansion and stabilisation [38]. Simultaneously

to pressure reduction, temperature decreases; this increases polymer viscosity and progressively fixes foam architecture, by solidification and re-crystallisation of the polymer. Rate of cooling has a significant effect on the porous structure: cooling too rapidly will fix small closed pores, whereas a very slow cooling will not allow freezing the structure, which will finally collapse. An intermediate must be found which allows interconnections to be created, while still stabilizing the morphology before it collapses. Foaming parameters tested are collected in Table 1.

2.2. Micro-computed tomography (μCT)

SEM and optical microscopy observations are limited to the construct surface. To get an idea of the 3D internal structure of foams, X-ray μCT was conducted on neat and composite polymer samples. For each foaming condition four cylinders were machined (diameter and height 8 mm), and scanned. Measurements were performed using an X-ray fan-beam-type tomograph (μCT 40, Scanco Medical AG, Switzerland), also referred to as a desktop μCT [30], at an energy of 50 kVp and a spatial resolution of 12 μm. From the resulting voxel data, a cubic volume of interest with side length of 5 mm (424 voxels) was selected in order to eliminate side effects induced by cylinder-sample machining. The grey-value images were segmented using a constrained 3D Gaussian filter ($\sigma = 1.2$, $s = 1$) to partly suppress the noise in the volumes, and a fixed threshold (19% of the maximum greyscale value) to extract foam matrix with a contrast adapted to all samples.

Quantitative analysis of the porosity and of the pore architecture can be obtained, based on the structural indices usually measured for bone samples [39]. Bone (scaffold) surface (BS) is determined by triangulation of the foam surface. Bone (scaffold) volume (BV) is calculated using tetrahedrons corresponding to the enclosed volume of the triangulated surface. Total volume (TV) is the global volume of the measured sample. Sample porosity ε^* (%) can therefore be calculated as (1−BV/TV). The specific surface available for pore adhesion is given by the bone surface-to-volume ratio (BS/BV). 3D images also enable the direct assessment of metric indices of feature sizes by actually measuring distances in the 3D space. Trabecular (pore wall) thickness (Tb.Th), and trabecular separation (Tb.Sp) or pore diameter can be computed. The structural degree of anisotropy (DA) is defined as the ratio between the maximal and minimal radius of the Mean Intercept Length (MIL) ellipsoid. Directional MIL is the average distance between two void/matrix interfaces in a given direction. The MIL ellipsoid is calculated by fitting the directional MIL to a directed ellipsoid using a least square fit.

2.3. Compression tests

Mechanical testing was carried out on a traction-compression device (UTS Test Systeme, Germany), with a cross-head speed of 0.5 mm/min. From a test, compressive modulus E^*, and elastic collapse stress σ_{el}^* can be determined. Samples were prepared with a special attention to obtain parallel surfaces, perpendicular to the testing direction.

Compression tests on cubic specimens ($10 \times 10 \times 10\,mm^3$) were used to evaluate foam mechanical *anisotropy* in compression. Experiments in three perpendicular directions allowed to determine three elastic moduli E_1^*, E_2^* and E_3^* (Fig. 1). For each foaming condition nine cubes were tested, three in each direction. Samples were made of neat PLA, and PLA loaded with 5 and 10 wt% HA or β-TCP. Anova analysis is carried out, using a significance level of 0.05, in order to evaluate if the differences between filler contents and testing directions are significant (XLstat software).

Viscoelasticity of foams was finally evaluated on cylindrical specimens (height and diameter of 8 mm), at three different cross-head speeds: 0.1, 0.25 and 0.5 mm/min (corresponding to strain rates of 0.0001, 0.0005 and 0.001/s, respectively). Cylinders were tested in the longitudinal or foaming direction. Samples made of PLA loaded with 2.5, 5 and 10 wt% HA or β-TCP were tested.

3. Results and discussion

Different processing conditions and ceramic contents resulted in a variety of porous structures. The

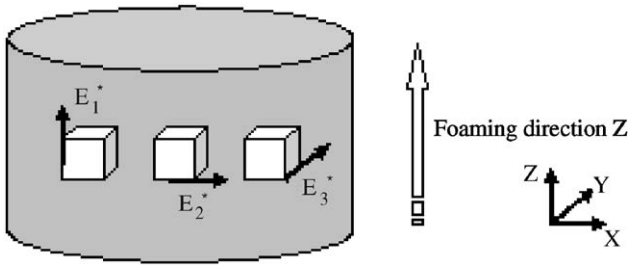

Fig. 1. Sample orientation in comparison with the foaming direction for mechanical anisotropy testing. Black arrows indicate direction of compression testing.

Table 1
Foaming conditions to prepare samples characterised by μCT and tested in compression

Condition	Materials	Saturation pressure P_{sat} (bar)	Depressurisation rate dP/dt (bar/s)	Cooling rate dT/dt (°C/s)
C1	PLA	150	6.7	2.8
C2	PLA	212	1.15	2.8
C3	PLA	243	20.4	5.2
C4_1HA (TCP)	PLA + 1%HA (TCP)	190	1.6	2.5
C4_5HA (TCP)	PLA + 5%HA (TCP)	190	1.6	2.5
C4_10HA (TCP)	PLA + 10%HA (TCP)	190	1.5	2.7

3D-macrostructure of these constructs was analysed by μCT, and their mechanical performance was assessed by compression testing.

3.1. 3D-macrostructure

The effects of foaming parameters on microcellular foam morphology have been analysed mostly with SEM and optical microscopic observations [40–42]. μCT characterisation was here conducted in order to determine the effect of foaming parameters (C1–C3) and ceramic content (C4) on neat and composite PLA foam macrostructures (Table 2 and Fig. 2). Conditions C2 and C4 presented similar processing parameters, which allowed a direct comparison between neat polymer and composite foams, independently of foaming conditions.

Condition C3 gave rise to a cellular structure with large, but few, pores and thick walls (Figs. 2e and f). The high saturation pressure could potentially induce a high pore density; however, high depressurisation rates led to a partial disintegration of the structure, with a few large pores in the centre, and closed pores on the outside, due to fast cooling.

Processing condition C2 resulted in a lower porosity and pore number than C1 although the saturation pressure was higher. This can be explained by a lower depressurisation rate which induced less nucleation and more coalescence, leading to fewer, but larger, pores (Figs. 2c and d).

C1 was the processing condition leading to the most suitable macrostructure for bone tissue engineering. In fact it had sufficient porosity, higher than 75%, the highest specific surface area and DA. The average pore diameter (0.40 ± 0.07 mm) was also in the defined range for bone [17,39]. All these characteristics were confirmed visually by the 3D reconstruction of the foam displaying elongated and interconnected pores (Fig. 2a). A 2D slice, perpendicular to the foaming direction, taken in the centre of the sample also confirmed pore interconnectivity and pore size (Fig. 2b).

Scaffold characteristics can be compared to similar values evaluated for trabecular bone. Using μCT, Hildebrand et al. [39] and Kabel et al. [43] measured morphometric parameters for human cancellous bones from different skeletal sites. They pointed out that large differences between inter and intra sites exist. For example a femoral head was characterised by a high bone volume fraction, thick trabeculae and a plate-like structure; whereas lumbar spine samples presented a low bone volume fraction, thin trabeculae and a rod-like structure. This explains the large variations given for trabecular bone in Table 2. All the foaming conditions tested led to foams with structural parameters in the range of those of cancellous bone, as displayed in Fig. 3 which compares three polymer foams and three different types of trabecular bones. Gas foaming therefore proved to be a flexible technique which enabled scaffolds to be processed with various macrostructures suitable for replacing different types of cancellous bones.

2D slices taken in the centre of a foam in three perpendicular planes confirmed anisotropy in foam morphology. A cross-section perpendicular to the foaming direction (Fig. 4c) displayed relatively regular and rounded pores, whereas cross-sections (Figs. 4a and b) containing the expansion direction revealed elongated pores along the foaming direction. This anisotropy was more or less pronounced depending on the density of nucleation and rate of cooling. A rapid cooling locked in a high number of spherical pores like in condition C3, whereas a slower cooling enabled pore elongation provided no coalescence occurred (C1).

The effects of ceramic content (0, 1, 5, and 10 wt%) and ceramic type (HA or β-TCP) on composite foam morphology were considered for a given foaming condition (Figs. 5 and 6). When ceramic content increased, porosity and specific surface decreased (Fig. 5a). The reduction of porosity was similar with β-TCP and HA, decreasing from 81% without ceramic to about 74% with 10 wt% of fillers. In the case of the specific scaffold surface BS/BV, the decrease was more pronounced with HA than with β-TCP. According to porosity changes, scaffold volume BV increased in a similar way with both ceramics. However, scaffold surface BS decreased faster with HA, where larger pores were created using higher filler content.

As far as pore diameter and wall thickness are concerned, they both increased when HA was added

Table 2
Effect of foaming conditions on neat PLA foam structural parameters

Condition	Porosity ε^* (%)	Bone surface to volume ratio BS/BV (1/mm)	Degree of anisotropy DA	Trabecular spacing Tb.Sp (mm)	Trabecular thickness Tb.Th (mm)
C1	84.81 ± 2.74	43.66 ± 2.72	1.53 ± 0.11	0.40 ± 0.07	0.08 ± 0.01
C2	80.78 ± 1.13	25.22 ± 1.14	1.34 ± 0.12	0.62 ± 0.07	0.13 ± 0.00
C3	87.80 ± 1.06	27.09 ± 3.01	1.29 ± 0.16	1.08 ± 0.01	0.12 ± 0.01
Trabecular bone [27,32]	52–96	7–34	1.1–2.38	0.45–1.31	0.08–0.28

Values are given as mean ± SD

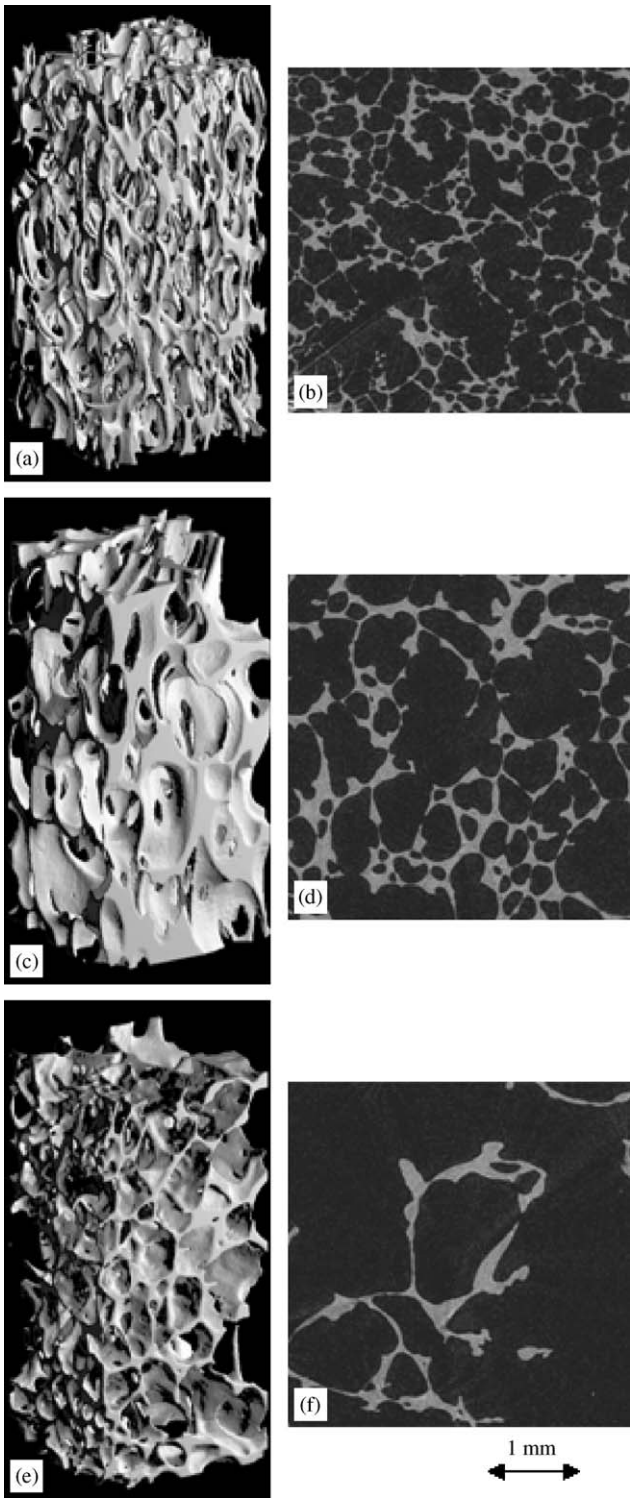

Fig. 2. The effect of foaming parameters on PLA foam morphology. 3D μCT reconstructions (a, c and e) and 2D slices perpendicular to the foaming direction Z (b, d, and f). (a,b) C1, (c,d) C2, and (e,f) C3.

to PLA, whereas they were relatively stable in the case of β-TCP (Fig. 5b). In a single cylindrical specimen these two parameters could vary significantly because of the pore diameter gradient created during foam expansion by different cooling rates in the core and the outside of the sample. With an increased amount of particles, pore walls became thicker, delimiting more closed pores. Anisotropy in foam morphology was also observed in the case of composite foams. The DA, in the range of 1.3–1.6, was similar with and without fillers, either HA or β-TCP. This characteristic did not seem to be significantly affected by the addition of fillers provided they were homogeneously dispersed in the polymer.

The main reason for these trends was the increase in viscosity of the matrix with the addition of fillers. Viscosity controlled foam expansion and stabilisation. A low viscosity will favour pore coalescence and pore wall rupture to create interconnections. On the contrary, an increased viscosity will limit pore growth and favour closed pores, therefore decreasing porosity, specific surface, and increasing pore wall thickness. Pore size is related to two main factors [44]. First there is competition between the gas diffusing out of the skin, which is therefore lost for pore growth, and the gas diffusing into nucleated pores. Second, the pore growth process is limited by the diffusion rate and the stiffness of the polymer matrix, depending in particular on matrix viscosity. Jin et al. [45] investigated the gas foaming of a liquid crystalline polymer (LCP)-filled polystyrene (PS). On the one hand, when LCP content increased, matrix viscosity increased, which tended to decrease pore size. On the other hand, an improvement of interfacial adhesion resulted in less gas loss and therefore an increase in pore size. The same competition between enhanced matrix viscosity and good interfacial adhesion occurred in our PLA/HA and PLA/β-TCP systems, finally leading to an increase in pore size. The effect of fillers on pore size in foam obtained by gas foaming is, however, still discussed. Zeng et al. [46] observed a decrease in pore size with higher nanoclay content in polystyrene. According to Chen et al. [47], pore size is also affected by filler size, depending on saturation pressure.

Variations of scaffold parameters were generally more significant with HA fillers than with β-TCP particles. The former tended to form aggregates and were generally less homogeneously dispersed in the matrix than the latter, which created zones with different viscosities and therefore different foaming behaviours. A 5 wt% filler content, and more preferably β-TCP, thus seems to be the higher limit to obtain a homogeneous and interconnected cellular architecture.

Filler distribution in the porous structure can also be visualised because of the difference in X-ray transmission of PLA and HA or β-TCP, displayed in grey and white, respectively, on the pictures (Fig. 7). During image treatment, contrast and threshold were adjusted but kept constant for all samples in order to be able to compare all structures. This choice may have eliminated some of the smallest particles, which explains why

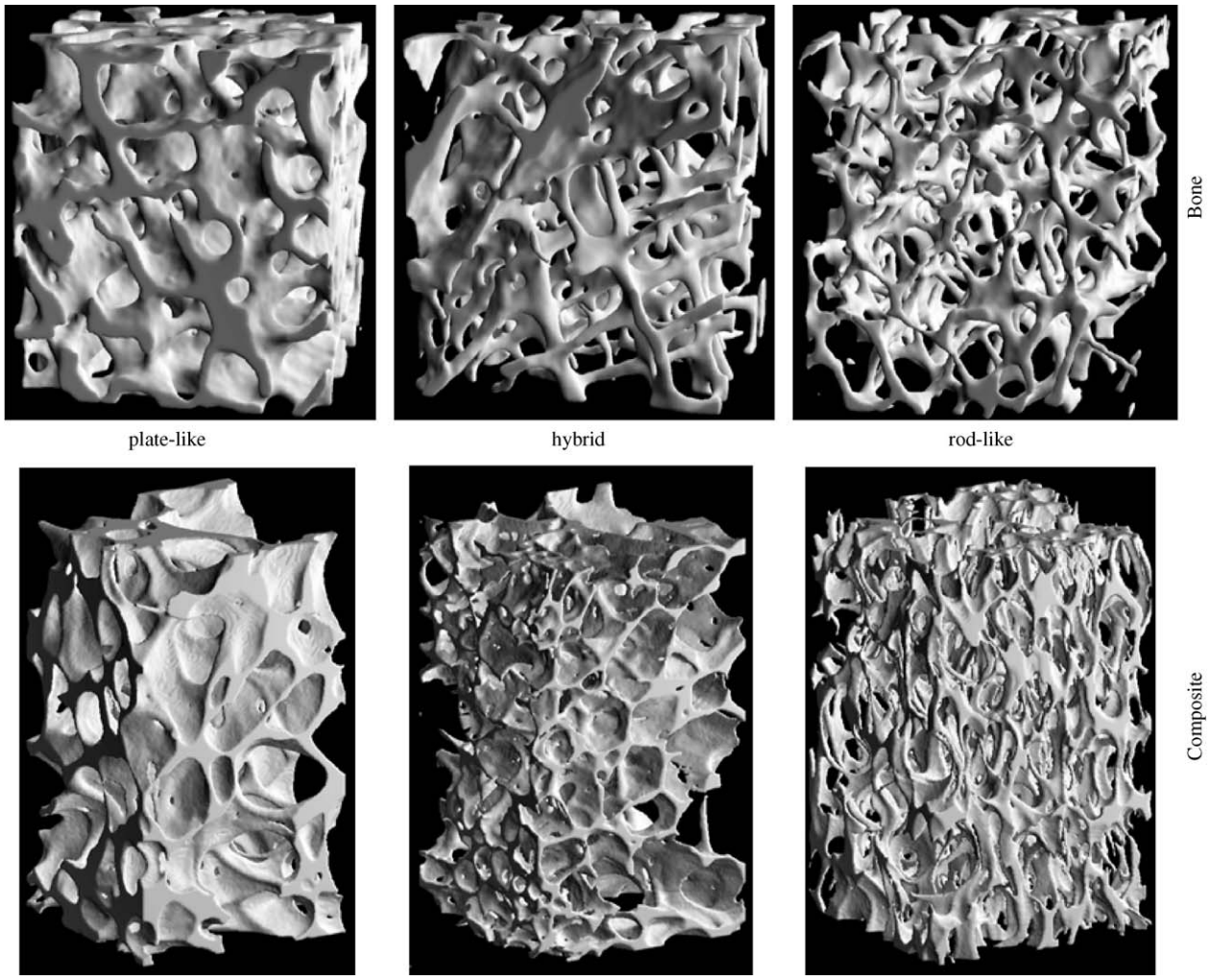

Fig. 3. Similarity of cancellous bone structures and polymer foam macrostructures.

micrometric β-TCP particles seemed to be more numerous than nanometric HA ones for the same ceramic content. However, the largest HA aggregates were still visible and were well dispersed in the pore walls. No ceramic rich zones were observed.

To summarise this part, knowing the structure of the bone which must be replaced, a set of processing parameters can be used for a given material formulation.

3.2. Mechanical behaviour: Anisotropy and viscoelasticity

Neat and composite polymer foams exhibited anisotropy in morphology with pores oriented along the foaming direction, as highlighted using the μCT study. Compression tests were carried out in order to ascertain whether they also presented anisotropy in their mechanical behaviour, induced by this anisotropic macrostructure. The results of compression experiments are presented in Fig. 8. In the parallel testing direction, composites with 5 wt% fillers were not found to have a significantly different modulus than the neat polymer. On the opposite, the moduli of 10-wt%-filled polymers differ significantly from both neat and 5-wt%-loaded polymers. Composite foams therefore tend to be more resistant than pure polymer foams. Ceramic fillers actually reinforced the skeleton matrix, which resulted in improved mechanical properties of the foams provided a homogeneous structure was prepared [29].

When looking at foam modulus, samples tested in compression parallel to the expansion direction were significantly more resistant than samples tested transversally to the foaming direction. No difference in moduli and elastic collapse stresses was noticed between the two transverse directions E_2^* and E_3^* (σ_{el2}^* and σ_{el3}^*). They were thus considered as one value E_T^* (σ_{elT}^*), an average of E_2^* and E_3^* (σ_{el2}^* and σ_{el3}^*). This anisotropic behaviour can therefore be qualified as transverse isotropic. Bone has a similar behaviour, presenting a higher mechanical resistance axially than transversally [48,49].

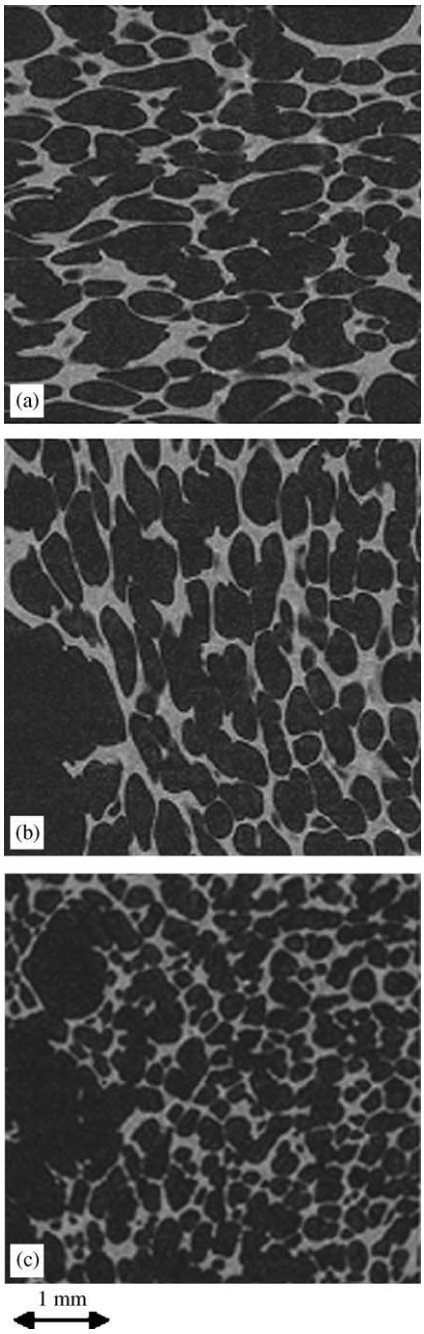

Fig. 4. Anisotropy in PLA foam morphology (C1) (a) *YZ* plane, (b) *XZ* plane, both parallel to the foaming direction *Z*; and (c) *XY* plane, perpendicular to the foaming direction *Z*.

This anisotropy was induced by the processing technique, giving rise to elongated and preferentially oriented pores. It was observed for all ceramic contents, from 0 to 10 wt% ceramic, either HA or β-TPC, and for different foaming conditions (C1 or C2). Modulus measured longitudinally could be up to 1.5 times higher than the transverse modulus. This ratio can be compared to the DA obtained by μCT, which was in a similar range (DA = 1.1–1.7). Anisotropy in

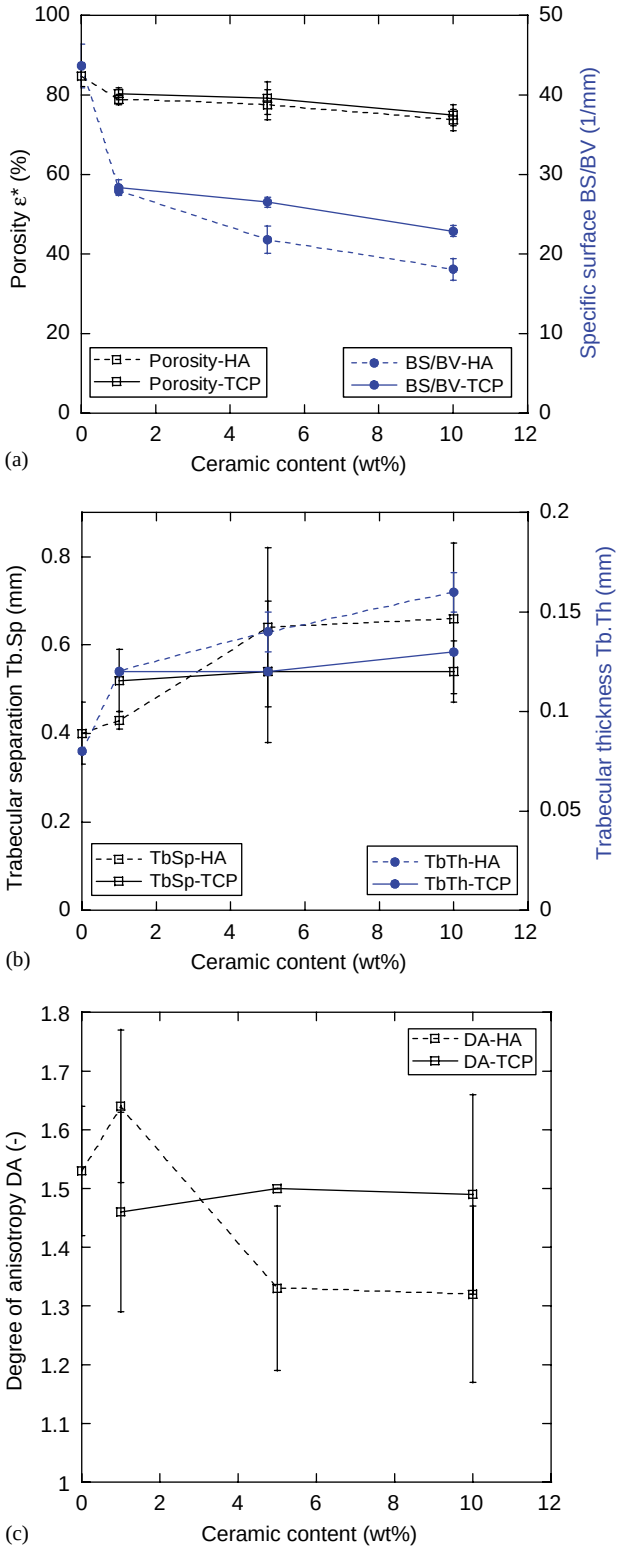

Fig. 5. The effect of ceramic content on (a) composite foam porosity ε^* and specific surface BS/BV, (b) pore size Tb.Sp (or trabecular separation) and trabecular thickness (Tb.Th), (c) degree of anisotropy of composite foams. Each point represents the mean of four samples. Error bars are standard deviations between these specimens.

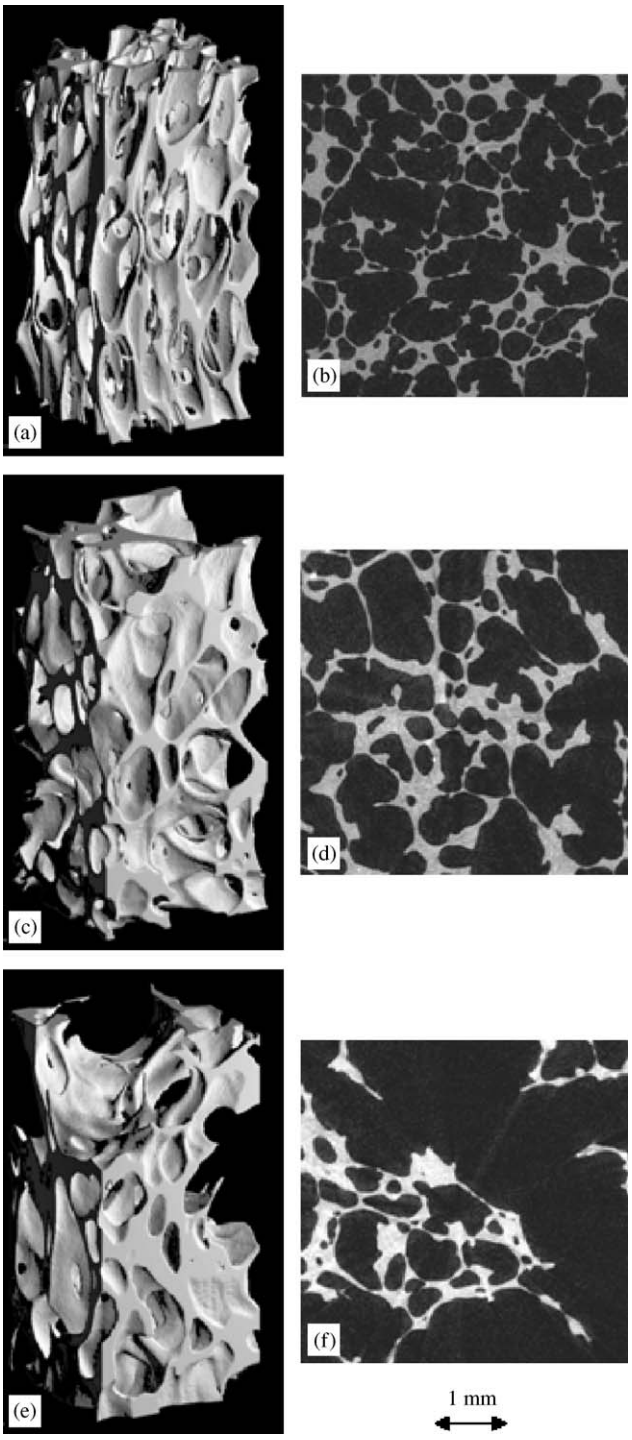

Fig. 6. The effect of HA content on composite foam morphology. 3D μCT reconstructions (a, c and e) and 2D slices perpendicular to the foaming direction Z (b, d, and f). (a,b) C4/1wt%HA, (c,d) C4/5 wt%HA, and (e,f) C4/10 wt%HA. Similar structures were observed with β-TCP fillers.

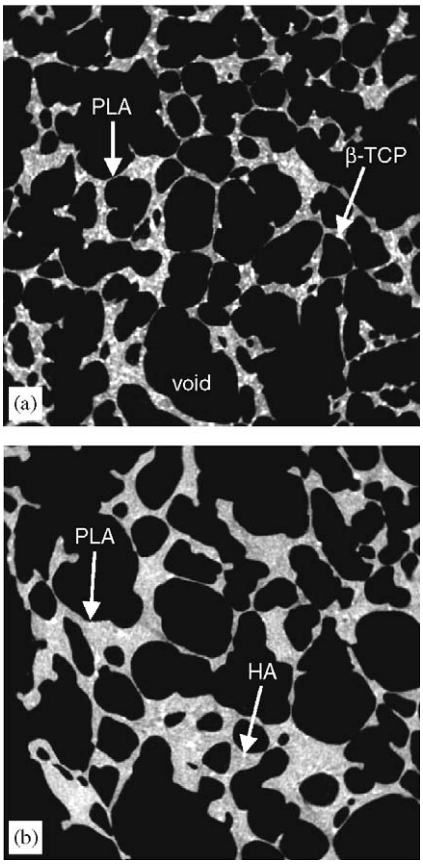

Fig. 7. Filler distribution: ceramic particles are homogeneously dispersed in pore walls (a) C4_10TCP, and (b) C4_10HA.

elastic collapse stress was less significant, with similar values measured longitudinally and transversally. Error bars were due to different densities and to different macrostructures because of the gradient structure of the main foam sample from which tested cubes were cut.

Gibson and Ashby [50] derived a model for anisotropic porous structures, which was experimentally verified [51,52]. For an anisotropic open pore foam, with struts of thickness t, and lengths h and l in the longitudinal and transverse directions, respectively, they calculated the ratios between longitudinal and transverse modulus (Eq. (1a)), and elastic collapse stress (Eq. (1b)):

$$\frac{E_L^*}{E_{\mathrm{T}}^*} = \frac{2(\mathrm{DA})^2}{1+(1/\mathrm{DA})^3}, \tag{1a}$$

$$\frac{\sigma_{\mathrm{elL}}^*}{\sigma_{\mathrm{elT}}^*} = \frac{n_{\mathrm{L}}^2}{n_{\mathrm{T}}^2}\frac{1}{\mathrm{DA}}, \tag{1b}$$

where $\mathrm{DA} = h/l$ is the structural DA, and n is the rotational stiffness of the strut.

These equations show that Young's modulus is more affected by anisotropy than elastic collapse stress, with a variation at least as marked as $(\mathrm{DA})^2$ for the former and only of (DA) for the latter. The weaker dependence of elastic collapse stress on the DA can be explained by two

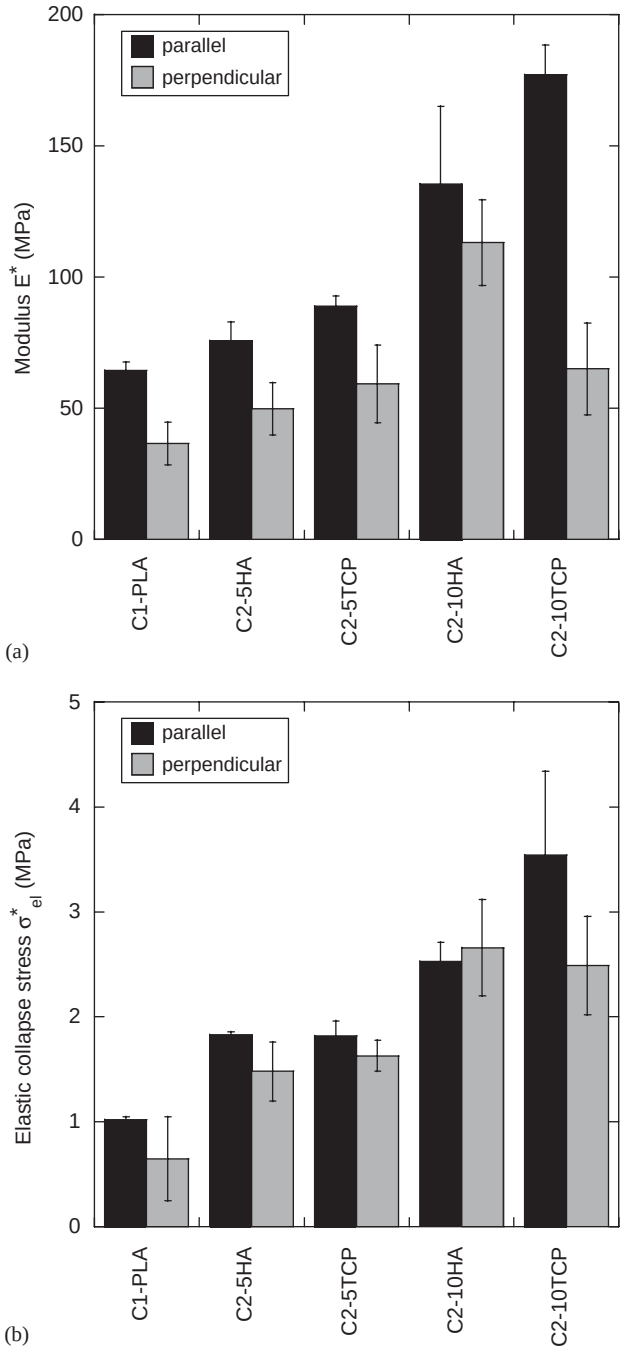

Fig. 8. The effect of testing direction on compressive properties of neat and composite polymer foams. (a) Modulus E^* and (b) Elastic collapse stress σ_{el}^*.

competing phenomena occurring during mechanical solicitation. Longer struts, if unconstrained at their ends, buckle more easily than shorter ones. However, the rotational constraints on longer struts are also greater than on shorter struts, which finally stabilise them.

In this study compressive modulus was as well shown to be more sensitive to anisotropy than elastic collapse stress. However, the moduli ratio E_L^*/E_T^* was similar to the morphological DA and not greater. This difference could be explained by a misalignment between the preferential pore orientation and the testing direction. Moreover, pore size was not homogeneous as in theoretical models, which induced locally higher stress and deformation, resulting in a lower global stiffness. Bone also behaves in an anisotropic way. Trabecular bone typically has a longitudinal modulus of 129.07 ± 49.48 MPa for a transverse one of 38.23 ± 20.18 MPa [48]. Few other studies have shown an interest in scaffold anisotropy. Using thermally induced phase separation, Ma and Zhang [53] manufactured microtubular scaffolds, with a higher longitudinal than transverse modulus (9.5 and 1.5 MPa, respectively). In the latter study, anisotropy was induced by the processing technique. On the other hand, Slivka et al. [54] created anisotropy by adding 2.5 mm PGA fibres to a PLGA foam, provided that fibres were oriented during processing. A compressive modulus in the axial direction up to six times higher than the transverse one was measured (32 and 5 MPa, respectively with 10 wt% fibres).

Anisotropy in morphology, described by μCT, was shown to induce anisotropy in compressive behaviour. This effect was especially pronounced with modulus, although it was less significant than theoretically expected from the Gibson and Ashby model.

Besides anisotropy, viscoelasticity is another specific property of natural bone. Bone was shown to have a viscoelastic behaviour, becoming stiffer under a higher strain rate solicitation [55]. Viscoelasticity of developed porous constructs was evaluated by compression at different strain rates. Results are presented in Fig. 9 with HA particles. The same trend was obtained with β-TCP fillers.

When a given strain rate is considered, the modulus and elastic collapse stress tended to increase with an increase in HA content up to 5 wt%. At higher contents, foams became fragile, as shown by the lower collapse stress with 10 wt% HA. When strain rate increased, higher moduli and collapse stresses were measured whatever the ceramic content. In log–log coordinates, the modulus increased linearly with strain rate. In semi-log coordinates the elastic collapse stress also increased linearly with strain rate. Carter et al. [56] derived a power law relating stress and strain rate $\sigma^* = k\dot{\varepsilon}^{\alpha}$. They evaluated $\alpha = 0.06$ for cancellous bone, whereas α values of 0.01–0.07 were determined for polymer and composite foams tested. The developed porous composite structures thus exhibited similar viscoelastic behaviour to that of natural bone. These viscoelastic measurements indicate a trend, and that the addition of fillers did not induce a loss of the viscoelastic behaviour.

Two factors contribute to the viscoelasticity of the cellular constructs. One is inherent to the solid

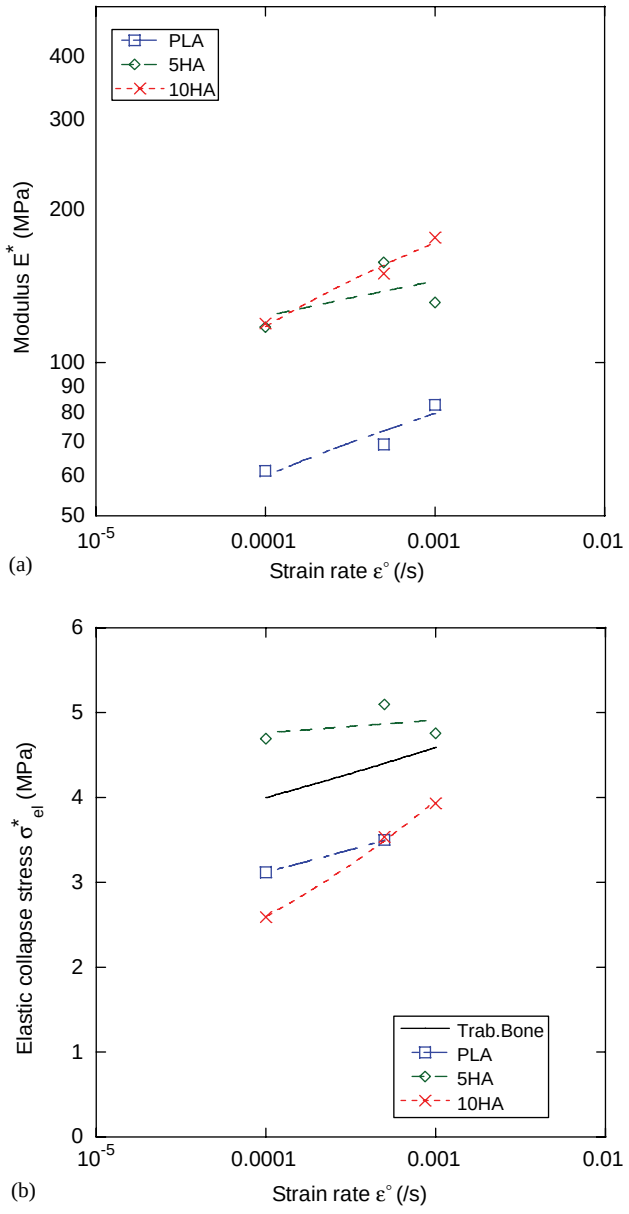

Fig. 9. The effect of strain rate on compressive properties of composite foams made of PLA, neat or filled with 5 and 10 wt% HA. (a) Modulus E^* and (b) Elastic collapse stress σ^*_{el}.

constituting the foam skeleton; and the second one is derived from the fluid which fills the pores. In this study, the latter was weak, pores being filled with gas only. Therefore, the main contribution to foam viscoelasticity was here due to the polymer, viscoelastic by nature. In physiological conditions, the cellular constructs will be filled by a liquid which will enhance the viscoelastic behaviour. Slivka et al. [54] have also highlighted the viscoelasticity of their fibre reinforced porous structures. With 10 wt% PGA fibres they obtained a linear relationship for modulus–strain rate and strength–strain rate curves, on log–log and semi-log coordinates, respectively.

4. Conclusions

μCT scans, applied to neat and composite polymer foams, evaluated histomorphometric parameters of 3D-constructs more precisely than with a 2D picture analysis. In particular, anisotropy, pore size variations and wall thickness were determined and compared to trabecular bone characteristics. 3D reconstructions of porous macrostructures were also obtained, allowing the internal cellular structure to be visualised. Processing conditions to obtain an optimum structure were determined.

Mechanical testing then demonstrated anisotropy in compressive properties and viscoelastic behaviour of neat and composite polymer foams prepared by supercritical gas foaming. Longitudinal modulus was up to 1.5 times higher than the transverse one, and was shown to increase with higher strain rates. This behaviour is similar to that of bone, with mechanical characteristics closer to bone properties than current polymer systems. Viscoelasticity and anisotropy, both in morphology and in mechanical properties, are promising characteristics for bone replacement. From a biological point of view, biocompatibility of human primary bone cells with composite scaffolds was demonstrated [57]. The latter study also relates the effect of the structure and properties of the scaffolds described here on cell proliferation and differentiation. Other properties are currently evaluated, such as scaffold changes during its resorption.

Acknowledgements

This work is financed by the Swiss National Science Foundation (FNRS No. 2100-066872.04.01) and the Lausanne Centre for Bone Tissue Engineering. The Dr. Robert Mathys Foundation is thanked for the donation of ceramic powders. T. Knecht is acknowledged for his help with the mechanical analysis.

References

[1] Service RF. Tissue engineers build new bone. Science 2000; 289(5484):1498–500.
[2] Hutmacher DW. Scaffolds in tissue engineering bone and cartilage. Biomaterials 2000;21:2529–43.
[3] Middleton JC, Tipton AJ. Synthetic biodegradable polymers as orthopedic devices. Biomaterials 2000;21(23):2335–46.
[4] Devin JE, Attawia MA, Laurencin CT. Three-dimensional degradable porous polymer-ceramic matrices for use in bone repair. J Biomater Sci Polymer Edn 1996;7(8):661–9.
[5] Marra KG, Szem JW, Kumta PN, DiMilla PA, Weiss LE. In vitro analysis of biodegradable polymer blend/hydroxyapatite composites for bone tissue engineering. J Biomed Mater Res 1999;47: 324–35.

[6] Laurencin CT, Lu HH. Polymer-ceramic composites for bone-tissue engineering. In: Davies JE, editor. Bone Engineering. 2000. p. 462–472
[7] Maquet V, Boccaccini AR, Pravata L, Notingher I, Jérôme R. Porous poly(α-hydroxyacid)/Bioglass^R composite scaffolds for bone tissue engineering. I: preparation and in vitro characterisation. Biomaterials 2004;25:4185–94.
[8] Wang M. Developing bioactive composite material for tissue replacement. Biomaterials 2003;24:2133–51.
[9] Bostrom RD, Mikos AG. Tissue engineering of bone. In: Atala A, Mooney D, editors. Synthetic biodegradable polymer scaffolds. Basel: Birkhaüser; 1997. p. 215–34.
[10] Brekke JH, Toth JM. Principles of tissue engineering applied to programmable osteogenesis. J Biomed Mater Res (Appl Biomater) 1998;43:380–98.
[11] Burg KJL, Porter S, Kellam JF. Biomaterial developments for bone tissue engineering. Biomaterials 2000;21(23):2347–59.
[12] Chapekar MS. Tissue engineering: challenges and opportunities. J Biomed Mater Res (Appl Biomater) 2000;53:617–20.
[13] Cima LG, Vacanti JP, Vacanti C, Ingber D, Mooney D, Langer R. Tissue engineering by cell transplantation using degradable polymer substrates. J Biomech Eng 1991;113:143–9.
[14] Freyman TM, Yannas IV, Gibson LJ. Cellular materials as porous scaffolds for tissue engineering. Prog Mater Sci 2001; 46:273–82.
[15] Peter SJ, Miller MJ, Yasko AW, Yaszemski MJ, Mikos AG. Polymer concepts in tissue engineering. J Biomed Mater Res (Appl Biomater) 1998;43:422–7.
[16] Freed LE, Vunjack-Novakovic G. Culture of organized cell communities. Adv Drug Delivery Rev 1998;33(1–2):15–30.
[17] Boyan BD, Hummert TW, Dean DD, Schwartz Z. Role of material surfaces in regulating bone and cartilage cell response. Biomaterials 1996;17:137–46.
[18] Ishaug SL, Crane GM, Miler MJ, Yasko AW, Yaszemski MJ, Mikos AG. Bone formation by three-dimensional stromal osteoblast culture in biodegradable polymer scaffold. J Biomed Mater Res 1997;36:17–28.
[19] Santos ARJ, Barbanti SH, Duek EAR, Dolder H, Wada RS, Wada MLF. Vero cell growth and differentiation on poly(L-lactic acid) membranes of different pore diameters. Artif Organs 2001;25(1):7–13.
[20] Calandrelli L, Immirzi B, Malinconico M, Orsello G, Volpe MG, Ragione FD, et al. Biocompatibility studies on biodegradable polyester-based composites of human osteoblasts: a preliminary screening. J Biomed Mater Res 2002;59:611–7.
[21] Mikos AG, Thorsen AJ, Czerwonka LA, Bao Y, Langer R. Preparation and characterization of poly(L-lactic acid) foams. Polymer 1994;35(5):1068–77.
[22] Whang K, Thomas CH, Healy KE, Nuber G. A novel method to fabricate bioabsorbable scaffolds. Polymer 1995;36(4):837–42.
[23] Whang K, Goldstick TK, Healy KE. A biodegradable polymer scaffold for delivery of osteotropic factors. Biomaterials 2000; 21(24):2545–51.
[24] Schugens C, Maquet V, Grandfils C, Jerome R, Teyssie P. Biodegradable and macroporous polylactide implants for cell transplantation. I. Preparation of macroporous polylactide supports by solid-liquid phase separation. Polymer 1996;37(6): 1027–38.
[25] Zhang R, Ma PX. Poly(α-hydroxyl acids)/hydroxyapatite porous composites for bone-tissue engineering. I. Preparation and morphology. J Biomed Mater Res 1999;44:446–55.
[26] Hile DD, Amirpour ML, Akgerman A, Pishko MV. Active growth factor delivery from poly(D,L-lactide-*co*-glycolide) foams prepared in supercritical CO_2. J Controlled Release 2000;66:177–85.
[27] Forman S, Kás J, Fini F, Steinberg M, Ruml T. The effect of different solvents on the ATP/ADP content and growth properties of HeLa cells. J Biochem Molecular Toxicol 1999; 13(1):11–5.
[28] Howdle SM, Watson MS, Whitaker MJ, Popov VK, Davies MC, Mandel FS, et al. Supercritical fluid mixing: preparation of thermally sensitive polymer composites containing bioactive materials. Chem Commun 2001;1:109–10.
[29] Mathieu L, Montjovent M-O, Bourban P-E, Pioletti DP, Månson J-AE. Bioresorbable composites prepared by supercritical fluid foaming. J Biomed Mater Res 2005, in press.
[30] Rüegsegger P, Koller B, Müller R. A microtomographic system for the non destructive evaluation of bone architecture. Calcif Tissue Int 1996;58:24–9.
[31] Müller R. Bone microarchitecture assessment: current and future trends. Osteoporos Int 2003;14(Suppl 5):S89–99.
[32] Müller R, Matter S, Neuenschwander P, Suter UW, Rüegsegger P. 3D micro-tomographic imaging and quantitative morphometry for the nondestructive evaluation of porous biomaterials. Mat Res Soc Symp Proc 1997;461:217–22.
[33] Zeltinger J, Sherwood JK, Graham DA, Müeller R, Griffith LG. Effect of pore size and void fraction on cellular adhesion, proliferation, and matrix deposition. Tissue Eng 2001;7(5): 557–72.
[34] Elliot JA, Windle AH, Hobdell JR, Eeckhaut G, Oldman RJ, Ludwig W, et al. In situ deformation of an open-cell flexible polyurethane foam characterised by 3D computed microtomography. J Mater Sci 2002;37:1547–55.
[35] Müller B, Beckmann F, Huser M, Maspero F, Székely G, Ruffieux K, et al. Non-destructive three-dimensional evaluation of a polymer sponge by micro-tomography using synchrotron radiation. Biomolecular Eng 2002;19:73–8.
[36] Lin ASP, Barrows TH, Cartmell SH, Guldberg RE. Microarchitectural and mechanical characterization of oriented porous polymer scaffolds. Biomaterials 2003;24:481–9.
[37] Mathieu L, Montjovent M-O, Bourban P-E, Pioletti DP, Zambelli P-Y, Applegate L, et al. Solvent-free processing of bioresorbable composite scaffolds for application to bone tissue engineering. In: TESI-ETES, Lausanne, 2004. p. 53.
[38] Mathieu L, Bourban P-E, Pioletti DP, Zambelli P-Y, Applegate L, Manson J-AE. Bioresorbable composite scaffolds processed by supercritical fluid foaming. In: 7th World Biomaterials Congress, 2004. Sydney: Australian Society for Biomaterials. p. 1276.
[39] Hildebrand T, Laib A, Müller R, Dequeker J, Rüegsegger P. Direct three-dimensional morphometric analysis of human cancellous bone: microstructural data from spine, femur, iliac crest, and calcaneus. J Bone Miner Res 1999;14(7):1167–74.
[40] Goel SK, Beckman EJ. Nucleation and growth in microcellular materials: supercritical CO_2 as foaming agent. AIChE J 1995; 41(2):357–67.
[41] Baldwin DF, Park CB, Suh NP. A microcellular processing study of poly(ethylene terephtalate) in the amorphous and semicrystalline states. Part I: microcell nucleation. Polym Eng Sci 1996;36(11):1437–45.
[42] Baldwin DF, Park CB, Suh NP. A microcellular processing study of poly(ethylene terephtalate) in the amorphous and semicrystalline states. Part II: cell growth and process design. Polym Eng Sci 1996;36(11):1446–53.
[43] Kabel J, Odgaard A, Rietbergen B, Huiskes R. Connectivity and the elastic properties of cancellous bone. Bone 1999;24(2):115–20.
[44] Park CB, Baldwin DF, Suh NP. Effect of the pressure drop rate on cell nucleation in continuous processing of microcellular polymers. Polym Eng Sci 1995;35(5):432–40.
[45] Jin W, Xingguo C, Mingjun Y, Jiasong H. An investigation on the microcellular structure of polystyrene/LCP blends prepared by using supercritical carbon dioxide. Polymer 2001;42: 8265–75.

[46] Zeng C, Han X, Lee LJ, Koelling KW, Tomasko DL. Polymer-clay nanocomposite foams prepared using carbon dioxide. Adv Mater 2003;15(20):1743–7.
[47] Chen L, Straff R, Wang X. Effect of filler size on cell nucleation during foaming process. In: ANTEC, 2001. p. 1732–1737.
[48] Williams JL, Lewis JL. Properties and an anisotropic model of cancellous bone from the proximal tibial epiphysis. J Biomech Eng 1982;104:50–6.
[49] Cullinane DM, Einhorn TA. Biomechanics of bone. In: Bilezikian JP, Raisz LG, Rodan GA, editors. Principles of bone biology. San Diego: Academic Press; 2002. p. 16–32.
[50] Gibson LJ, Ashby MF. Cellular solids—structure and properties. Oxford: Pergamon Press; 1988.
[51] Gupta S, Watson B, Beaumont PWR, Ashby MF. Final year project. Cambridge: Cambridge University Engineering Department; 1986.
[52] Huber AT, Gibson LJ. Anisotropy of foams. J Mater Sci 1988;23(8):3031–40.
[53] Ma PX, Zhang R. Microtubular architecture of biodegradable polymer scaffolds. J Biomed Mater Res 2001;56:469–77.
[54] Slivka MA, Leatherbury NC, Kieswetter K, Niederauer GG. Porous, resorbable, fibre-reinforced scaffolds tailored for articular cartilage repair. Tissue Eng 2001;7(6):767–80.
[55] Nordin M, Frankel VH. Biomechanics of bone. In: Nordin M, Frankel VH, editors. Basic biomechanics of the musculoskeletal system. Philadelphia, London: Lea & Febiger; 1989.
[56] Carter DR, Hayes WC. Bone compressive strength: the influence of density and strain rate. Science 1976;194:1174–6.
[57] Montjovent M-O, Mathieu L, Hinz B, Applegate L, Bourban P-E, Zambelli P-Y, et al. Biocompatibility of bioresorbable PLA composite scaffolds with human fetal bone cells. Tissue Eng 2005;11:in press.